Journal of Materials Chemistry A

PAPER

Cite this: J. Mater. Chem. A, 2015, 3, 23106

Synergistic synthesis of quasi-monocrystal CdS nanoboxes with high-energy facets†

Li-Li Han,[ad] Sergei A. Kulinich,[bc] Yang-Yang Zhang,[a] Jin Zou,[e] Hui Liu,[f] Wei-Hua Wang,[g] Hui Liu,[g] Hao-Bo Li,[g] Jing Yang,[a] Huolin L. Xin,[d] Shi-Zhang Qiao[ah] and Xi-Wen Du*[a]

Received 17th July 2015
Accepted 2nd September 2015

DOI: 10.1039/c5ta05472a

www.rsc.org/MaterialsA

Hollow nanostructures with a highly oriented lattice structure and active facets are promising for catalytic applications, while their preparation *via* traditional approaches contains multiple steps and is time and energy consuming. Here, we demonstrate a new one-step strategy involving two complementary reactions which promote each other; it is capable of producing unique hollow nanoparticles. Specifically, we apply synergic cooperation of cation exchange and chemical etching to attack PbS nanosized cubes (NCs) and produce CdS quasi-monocrystal nanoboxes (QMNBs) which possess the smallest dimensions reported so far, a metastable zinc-blende phase, a large specific surface area, and particularly high-energy {100} facets directly visualized by aberration-corrected scanning transmission electron microscopy. These properties in combination allow the nanoboxes to acquire exceptional photocatalytic activities. As an extension of the approach, we use the same strategy to prepare Co_9S_8 and $Cu_{7.2}S_4$ single-crystal hollow nanooctahedrons (SCHNOs) successfully. Hence, the synergic reaction synthesis strategy exhibits great potential in engineering unique nanostructures with superior properties.

Introduction

Hollow nanostructures possess a large specific area, unique exposed crystal planes and tunable energy levels, which make them highly attractive for applications in various fields related to catalysis, energy storage and conversion, biomedicine, *etc*.[1–3] So far, most common synthetic routes to prepare hollow nanostructures typically involve multiple steps. For example, template-based synthesis of hollow nanostructures is usually comprised of three steps: (i) template preparation, (ii) shell growth on the template surface, and (iii) template elimination.[4,5] Typically, such multi-step processes are time- and energy-consuming. An alternative way is to combine two or more processes and run them simultaneously in one system. Such a synthetic route, hereafter named "synchronous reactions", has succeeded in the synthesis of hollow microspheres,[6] nanoboxes,[7,8] nanocages,[9,10] nanoframes,[11] nanotubes,[12] complex 3-dimensional nanostructures,[13] and yolk–shell nanostructures.[5] Even so, the component reactions used in most synchronous approaches typically work separately rather than complement each other. As a result, their many products have relatively low quality with polycrystallinity, non-uniform shell thickness and damaged shells.[9,14] Moreover, only a few studies about the preparation of non-spherical hollow particles were reported because of their structural instability.[15,16]

It is anticipated that synchronous approaches can be further improved by carefully selecting complementary component reactions, so that they can promote each other to engineer complex nanostructures with superior properties. This strategy is defined as "synergistic reactions" to distinguish it from the commonly used synchronous reactions. It is noted that, on one hand, cation exchange is well known as a powerful approach for synthesizing nanostructures through cation substitution within the anion frame, in which the product can generally preserve the crystal structure of templates, even at the nanoscale.[17,18] On the other hand, chemical etching is a common practice to remove the template or inner material and produce hollow nanostructures.[5] When these two reactions collaboratively attack single-crystal nanoparticles, chemical etching may promote the cation exchange by creating new exchange sites

[a]School of Materials Science and Engineering, Tianjin University, Tianjin 300072, China. E-mail: xwdu@tju.edu.cn

[b]Institute of Innovative Science and Technology, Tokai University, Hiratsuka, Kanagawa 259-1292, Japan

[c]School of Engineering and Applied Science, Aston University, Birmingham, B4 7ET, UK

[d]Center for Functional Nanomaterials, Brookhaven National Laboratory, New York 11973, USA

[e]Materials Engineering and Centre for Microscopy and Microanalysis, The University of Queensland, QLD 4072, Australia

[f]School of Material Science and Engineering, Hebei University of Technology, Tianjin 300130, China

[g]Department of Electronics, College of Electronic Information and Optical Engineering, Nankai University, Tianjin 300071, China

[h]School of Chemical Engineering, The University of Adelaide, SA 5005, Australia

† Electronic supplementary information (ESI) available: Detailed synthetic procedures, characterization methods, calculation and additional experimental results. See DOI: 10.1039/c5ta05472a

This journal is © The Royal Society of Chemistry 2015

and decreasing the diffusion length, which is favorable for the preparation of hollow structured nanoparticles. Unfortunately, there has not been any report about the synthesis of hollow nanoparticles using this strategy.

Cadmium sulfide (CdS), an important semiconductor with a band gap of 2.4 eV at room temperature, has attracted considerable interest in photocatalysis,[19–22] light-emitting diodes,[23] solar cells,[24] and other optoelectronic applications.[25] Many synthesis methods, such as electrochemical deposition,[26] solvothermal (hydrothermal) synthesis,[22,27] chemical vapor deposition (CVD)[28] and microwave radiation,[29] have been developed to prepare CdS nanostructures, among which are irregularly shaped nanoparticles,[19,30] nanotubes,[31] nanowires,[22] nanorods,[32] nanobelts,[33] *etc.* Nevertheless, the reported CdS catalysts usually expose low-energy facets due to surface energy minimization during the crystalline growth processes,[34–36] which limits their catalytic performance.[37,38] Thus, so far, there has not been any general approach for the synthesis of cubic CdS with an ultrafine size, highly active surfaces and a large specific surface area for advanced photocatalytic applications.

In the present work, applying the synergic reactions of chemical etching and cation exchange on PbS nanocubes (NCs), we for the first time obtained the smallest ever reported CdS quasi-monocrystal nanoboxes (QMNBs) (14 nm in length and 2.5 nm-thick walls) with a uniform size and uncommon cubic structure. Aberration-corrected scanning transmission electron microscopy (STEM) shows that the prepared CdS QMNBs are primarily terminated with {100} facets. Density function theory (DFT) calculations suggest that, among various low index planes of the zinc-blende CdS phase, {100} planes exhibit the highest surface energy (even an order of magnitude larger than that of {110} planes). Thus, CdS QMNBs with high energy {100} facets demonstrate superior photocatalytic efficiency over CdS nanoparticles (NPs) with the same quantity but an even larger specific surface area, which makes the new material very promising for catalytic applications. The new strategy is further extended to successfully prepare Co_9S_8 and $Cu_{7.2}S_4$ single-crystal hollow nanooctahedrons (SCHNOs), demonstrating that it is a useful method to develop new hollow nanostructures.

Experimental section

Materials synthesis

The preparation approach is depicted in Scheme 1 and the details are given in the ESI.† The 15.6 nm-sized PbS NCs were obtained by a hot-injection method. The procedures were mainly the same as previously reported in the literature with only slight modifications.[39] 54 mg of sulfur powder dissolved in 5 mL of oleylamine (OAm) was injected into the three-neck flask with 0.56 g of $PbCl_2$ dissolved in 10 mL of OAm at 220 °C. The mixture was aged for 1 h, resulting in a black colloidal solution. After cooling down, the black solution was centrifuged, washed with ethanol and finally dried in a vacuum desiccator. CdS nanoboxes were prepared according to the following procedures. First, 0.2658 g of PbS NCs was dispersed in 100 mL of oleic acid (OA) to obtain a suspension. Then, 3 mL of the suspension was mixed with 15 mL of 0.5 M cadmium acetate dissolved in OA. After the reaction proceeded at 180 °C for a given period of time (2–35 min) in the three-neck flask, the mixture was momentarily cooled down to room temperature and centrifuged to separate the deposit. Finally, the product was washed with ethanol several times prior to further characterization. The preparation procedures for Co_9S_8 and $Cu_{7.2}S_4$ SCHNOs were the same as described above for the preparation of CdS QMNBs except that 0.05 M Co(II) acetate tetrahydrate and 0.05 M Cu(II) acetate monohydrate were used instead of 0.5 M Cd acetatetrihydrate and the reaction temperatures were set at 300 °C and 150 °C, respectively.

Characterization of materials

Phase analysis was carried out by X-ray diffractometry (XRD, Bruker D8 advance instrument). The product morphology was determined by transmission electron microscopy (TEM, FEI Technai G2 F20, equipped with a field emission gun operating at 200 kV). The composition was analyzed with an Oxford INCA energy-dispersive spectroscopy (EDS) module attached to the TEM microscope. Atomic-resolution annular dark-field (ADF) and annular bright-field (ABF) images were performed with an Enfina spectrometer on a Hitachi 2700C STEM. A Hitachi S-4800 SEM was used to analyze the NP shape and surfaces. The light absorption spectra of the samples were examined using a Hitachi 3010 UV-vis absorption spectrometer. A solar simulator (Sciencetech, SS150) was used as the light source for photocatalysis experiments. Nitrogen sorption measurements were performed at 77 K using an autosorb iQ instrument (Quantachrome, US).

Surface energy calculations of zinc-blende CdS

The DFT calculations of the surface energies were performed using the Vienna *ab initio* simulation package (VASP) with choosing the generalized-gradient approximation (GGA) of Perdew, Burke and Ernzerhof (PBE) for the exchange-correlation function.[40] The Monkhorst–Pack *k*-point grids of $(8 \times 8 \times 8)$ and $(8 \times 8 \times 1)$ were adopted for the bulk and slab calculations, respectively. All the neighboring slabs were separated by a 15 Å vacuum space. In the geometry optimizations, the positions of all the atoms were fully relaxed until the force on each atom converged to 0.01 eV $Å^{-1}$. For the bulk CdS, the optimized lattice constant was 5.832 Å, which agreed well with the experimental values of 5.795 Å or 5.830 Å.[41] For the (100), (110) and (111) slab models, each slab contained 16 layers with 16 Cd and 16 S atoms. The two top layers and two bottom layers were fully relaxed while the other layers were fixed.

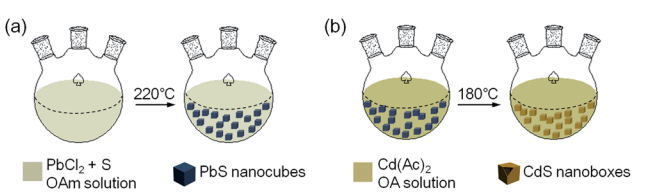

Scheme 1 Schematic illustration of (a) synthesis of PbS nanocube templates and (b) one-step transformation into CdS nanoboxes.

The surface energies were calculated using the following formula:

$$E_{surface} = 1/2[E_{slab} - nE_{bulk}]/A$$

where A is the surface area of the slab model, E_{bulk} is the bulk energy per unit cell, and E_{slab} is the energy of each slab model, which contains n bulk unit cells. The constant 1/2 indicates that two surfaces of the slab model are taken into account.

Results and discussion

The PbS NCs, used as templates, exhibit a uniform cubic morphology and narrow size distribution centered around 15.6 nm (Fig. 1a). Upon reacting with OA-dissolved $Cd(Ac)_2$ at 180 °C, the morphology of the PbS NCs changes with time. After 10 min, a light contrast preferably appears at the vertexes and edges of the NCs, and tiny holes can be found on the surfaces of some PbS NCs (Fig. 1b), indicating that etching initiates locally rather than evenly over the entire surface. The small holes grow bigger as the reaction time increases to 20 min (Fig. 1c). The interior of PbS NCs is almost etched away completely when the reaction reaches 35 min, and most of the solid PbS NCs are found to be transformed into well-defined nanoboxes. The nanoboxes have a mean outer size of ~14 nm with a wall thickness of 2.5 nm (Fig. 1d), thus being the smallest compound nanoboxes ever reported. Their specific surface area, 63 m^2 g^{-1}, estimated from the Brunauer, Emmett and Teller (BET) measurement, is by far larger than that of PbS NCs (0.76 m^2 g^{-1}) (Fig. S1†). The composition and structure of the PbS NC templates over the reaction duration were investigated by means of EDS and XRD. As clearly seen in Fig. 1e and f, PbS peaks gradually decrease while those of CdS increase with the reaction time. When the reaction time reaches 35 min, PbS almost disappears, and the main product is the zinc-blende structured CdS.

The atomic surface structure of the obtained CdS nanoboxes is revealed by aberration-corrected STEM. As shown in Fig. 2a, the product particle is a quasi-monocrystal nanobox (QMNB) with well oriented lattices and a few small-angle grain boundaries, which is also shown in the high resolution TEM (HRTEM) image in Fig. S2.† Due to the relatively low atomic number of sulfur compared to cadmium, sulfur columns cannot be directly imaged by the traditional annular dark-field STEM imaging. To visualize the sulfur column, we employed two new optical geometries, *i.e.* the annular bright-field (ABF) and the ultra-low-angle annular dark-field (ULAADF) STEM images; the simultaneously acquired atomic-resolution images taken along the [001] zone axis (Fig. 2b and c) clearly depict sulfur and cadmium positions on the surface of the CdS QMNBs. From the images, the projected zinc-blende unit cell is composed of a periodic square array of Cd columns surrounded by S columns, which is consistent with ABF and ULAADF simulations (insets of Fig. 2b and c). {100}-determined facets and small steps on the surface are observed in Fig. 2b and c, which clearly shows the {100} facet exposure.

To obtain CdS nanoboxes with larger {100} facets, we then employed 50 nm-sized PbS NCs as the template. The morphology evolution of the products was found to follow the same mode as that for 15.6 nm-sized PbS NCs according to the observation of SEM and TEM images (Fig. S3†), and QMNBs with 50 nm of sizes and exposed {100} planes were finally produced. Moreover, elemental mapping and line-scan were performed to reveal the elemental distribution in the intermediate product obtained after 10 min of reaction (its morphology is presented in Fig. S3c and d†). The results shown in Fig. S4† demonstrate that Pb atoms are absent at the cavity region of the hollow particle, while Cd atoms are evenly distributed throughout the whole particle, suggesting the formation of a homogenous CdS shell around the cavity.

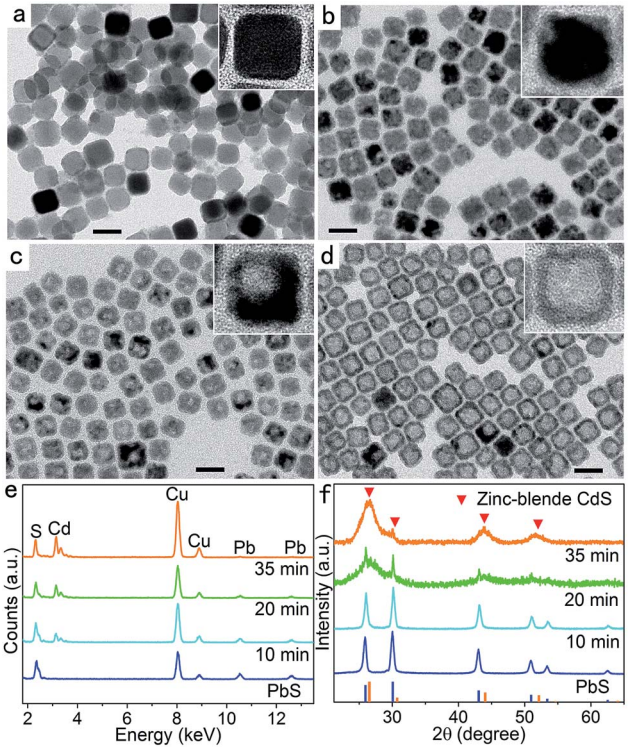

Fig. 1 Evolution from PbS nanocubes to CdS nanoboxes. TEM images of the products obtained at 180 °C after (a) 0 min, (b) 10 min, (c) 20 min and (d) 35 min reaction. The scale bar is 20 nm. (e) and (f) are EDS spectra and XRD patterns, respectively, of the products after different reaction times.

As a comparison, single-reaction or two-step synthesis generates products distinct from the QMNBs prepared *via* the synergic reactions. Firstly, PbS/CdS core/shell NCs (CSNCs) are produced by applying only cation exchange in a mixed solvent (9 mL of OA and 9 mL of ODE) under N_2 flow for 10 min at 250 °C, with PbS cores showing atomically sharp {110} edges (Fig. 3a and b). The *ab initio* calculations indicate that the {111}PbS/{111}CdS and {110}PbS/{110}CdS interfaces are more stable than the {100}PbS/{100}CdS one (see Fig. 3c and Table S1†), suggesting that cation exchange proceeds anisotropically.

Secondly, PbS NCs shrink into quasi-spheres after being solely etched in OA saturated with air (Fig. S5†), while they remain intact after being heated in OA with N_2 as the protective gas (Fig. S6†), indicating that air (oxygen) is essential for chemical etching. Thirdly, PbS/CdS CSNCs prepared by cation

This journal is © The Royal Society of Chemistry 2015

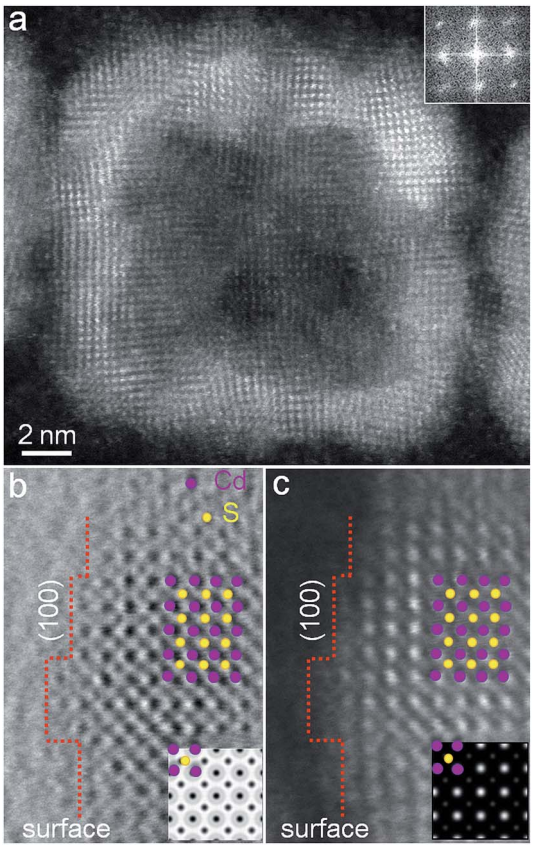

Fig. 2 Revealing atomic surface structure of CdS QMNBs. (a) Atomic-resolution ADF-STEM image of one QMNB. The inset is a corresponding FFT pattern. (b) Atomic-resolution ABF-STEM and (c) atomic-resolution ULAADF-STEM images of the surface structure of CdS QMNBs along the [001] zone axis after Richardson–Lucy deconvolution. The exposed facet profiles are outlined by red dotted lines. The insets show ABF and ULAADF simulations, respectively. The sulfur columns can be directly visualized in the ABF-STEM and ULAADF-STEM images.

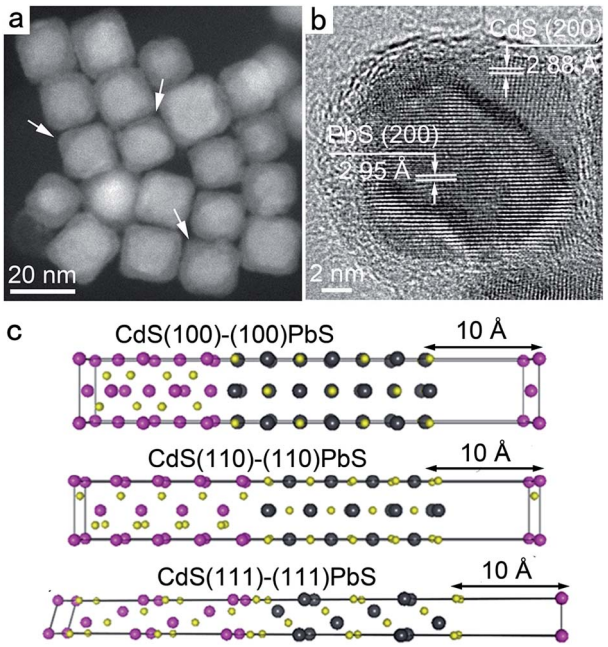

Fig. 3 Products of component reactions and the calculation of interface energies. (a) and (b) are high-angle-annular-dark-field scanning transmission electron microscopy (HAADF-STEM) and HRTEM images of PbS/CdS core/shell nanostructures obtained *via* cation exchange alone, respectively. The white arrows in (a) indicate the CdS areas. (c) Side views of three different CdS/PbS interfaces: (100)/(100), (110)/(110) and (111)/(111), with pink, gray and yellow balls representing Cd, Pb and S atoms, respectively. A vacuum layer with a thickness of 10 Å was added during calculations to avoid the interactions between the PbS surface and the opposite CdS surface atoms.

exchange under N_2 flow (Fig. S7a†) were chemically etched into the CdS debris with irregular hollow or compact structures (see Fig. S7b and c†), demonstrating that the stepwise synthesis cannot produce high-quality CdS QMNBs.

To elucidate the mechanisms of the CdS QMNB formation, we systematically investigated intermediate products using HRTEM (Fig. 4a–f). The PdS templates exhibited high crystallinity (Fig. 4a). As the reactions proceeded, first cation exchange started at the NC vertexes and edges (Fig. 4b). Afterwards, small jagged cavities appeared on the {100} surfaces of PbS NCs (Fig. 4c). The cavities then expanded into the PbS NCs while the transformed CdS shells kept intact (Fig. 4d). Interestingly, the cation exchange did not occur to a large extent on the front wall of the freshly formed cavity (Fig. 4d and e). As a result, the expansion of the cavity guided cation exchange along the NC inner surface and led to the formation of a uniform CdS shell (Fig. 4d and e, see discussion below). Finally, the PbS core was etched out and a QMNB was obtained (Fig. 4f).

Based on the above HRTEM observations, the transition from PbS NCs to CdS QMNBs can be schematically illustrated, as shown in Fig. 4g: (i) at the very beginning, cation exchange takes place very rapidly and proceeds in an anisotropic fashion.[42,43] Since the NC vertexes and edges along the ⟨111⟩ and ⟨110⟩ directions are more active compared with the stable {100} planes, cation exchange preferably takes place in these regions first, and then saturates when a formed CdS layer reaches its equilibrium thickness, which is temperature-dependent and related to the interdiffusion free path (L) of cations on the {111} planes.[43] (ii) As the processes proceed, chemical etching attacks the exposed {100} surfaces of PbS NCs, where it is more likely to succeed at a defect site, first producing a pin-hole. In turn, the hole edges become active sites and can be exchanged with Cd^{2+}cations. Subsequently, cation exchange proceeds rapidly and stops as a CdS layer reaches its threshold thickness. (iii) As time elapses, chemical etching proceeds inwards and laterally, gradually expanding the hole into a cavity. Meanwhile, cation exchange is prohibited at the spherical front wall of the cavity, because its shape, unlike the vertexes and edges, is not favorable for cation diffusion. On the other hand, the spherical frontier keeps dissolving and moving on, thus creating very unfavorable conditions for the nucleation and steady growth of CdS on its surface. Being intrinsically a nucleation-growth process,[43] the cation exchange cannot proceed on such an "unstable" surface. In contrast, the NC wall area undergoes severe cation exchange as now the CdS around the hole acts as

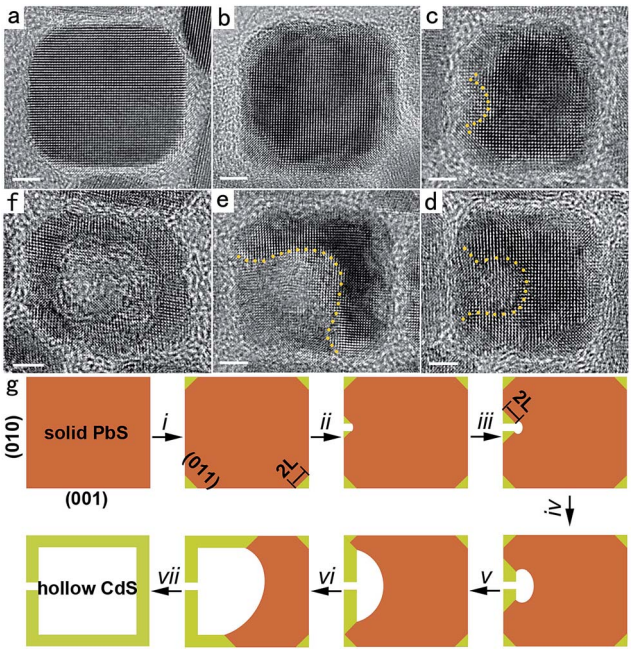

Fig. 4 Structural evolution from PbS nanocubes to CdS QMNBs as synergic reactions proceed. (a)–(f) HRTEM images of products representing different stages of transformation from PbS NCs to hollow CdS nanoboxes. The scale bar is 3 nm. (g) Schematic cross sectional profiles for the evolution of a PbS NC to a CdS nanobox as viewed along the ⟨100⟩ direction.

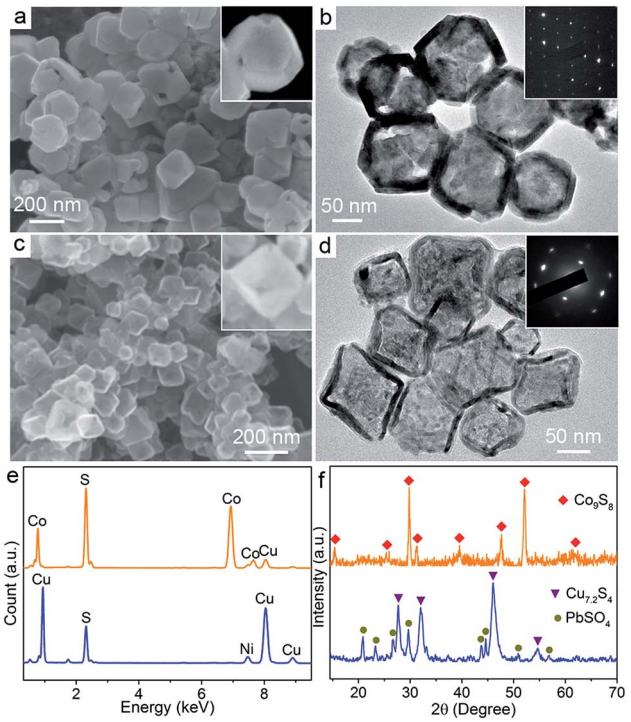

Fig. 5 Single-crystalline hollow Co_9S_8 and $Cu_{7.2}S_4$ nanooctahedrons synthesized *via* the reaction of PbS nanooctahedrons with OA-dissolved $Co(Ac)_2 \cdot 4H_2O$ and $Cu(Ac)_2 \cdot H_2O$, respectively. (a) SEM and (b) TEM images of Co_9S_8; (c) SEM and (d) TEM images of $Cu_{7.2}S_4$; (e) EDS spectra and (f) XRD patterns of the products presented in panels (a)–(d). The insets of (b) and (d) are SAED patterns of one particle. In EDS spectra of (e), Cu signals in Co_9S_8 and Ni signals in $Cu_{7.2}S_4$ originate from the copper grid and the nickel grid, respectively.

stable nuclei and the cation interdiffusion can proceed easily there, from both outside and inside. As a result, the CdS area grows with the expansion of the cavity. In particular, the thickness of the CdS layer remains constant in accordance with the interdiffusion free path length of cations. (iv–vii) Next, chemical etching continues to hollow out the PbS NC, and the exchanged CdS walls advance along the PbS NC contour, guiding cation exchange to a complete, uniform, and single-crystal CdS shell. Eventually, this results in the formation of a CdS QMNB.

To extend the synergic reaction synthesis approach, we then employed Co^{2+} and Cu^{2+} cations instead of Cd^{2+} to attack PbS octahedron templates. It was found that Co_9S_8 and $Cu_{7.2}S_4$ single-crystalline hollow nanostructures were respectively obtained (Fig. 5). SEM and TEM images (Fig. 5a–d) demonstrate that both products are hollow nanooctahedrons with single-crystal shells, which is confirmed by SEAD patterns in the insets of Fig. 5b and d. EDS (Fig. 5e) and XRD (Fig. 5f) results reveal that the rock-salt PbS templates were consumed completely, and the obtained hollow nanooctahedrons are rock-salt Co_9S_8 and $Cu_{7.2}S_4$.

The prepared CdS QMNBs exhibit unique {100} facets and a large specific surface area (63 $m^2\ g^{-1}$) which are of great benefit to photocatalytic properties. First, density function theory (DFT) calculations were made to determine the surface energy of CdS QMNBs. Among low-index planes {100}, {110} and {111} of the zinc-blende CdS phase, the {100} planes exhibit the highest surface energy (0.02657 eV $Å^{-2}$), much larger than those of {110} (0.00255 eV $Å^{-2}$) and {111} (0.01610 eV $Å^{-2}$) planes (Fig. 6a). Therefore, it is expected that the CdS QMNBs with exposed {100} facets would possess high dye adsorption capability and photocatalytic activity.[44–46] Accordingly, we tested the photocatalytic performance of CdS QMNBs after OA was stripped from their surface (Fig. S8†), by adopting the photodegradation of methylene blue (MB) as the probe reaction.[47] Two samples, CdS NPs obtained by synchronous reactions (see ESI and Fig. S9† for details) and CdS debris synthesized by stepwise reactions (see ESI and Fig. S7b–d† for details), were used as references. As shown in Fig. 6b, almost no degradation of methylene blue solution happened with CdS QMNBs in darkness. Under light irradiation, the QMNBs exhibited superior photodegradation efficiency compared to the CdS NPs and debris with the same quantity.

To evaluate the activity of CdS QMNBs quantitatively, the apparent reaction rate constant per unit surface area (k_s) of MB degradation was calculated (see ESI†), and the results are summarized in Table S2.† The k_s values of the CdS debris, NPs and QMNBs are 0.010068, 0.007394 and 0.03681 $min^{-1}\ m^{-2}$, respectively. Apparently, the k_s value of QMNBs with exposed {100} facets is 5 times that of NPs with an irregular surface. Therefore, the high degradation rate of QMNBs could be ascribed to their unique exposed facets. On one hand, the {100} facets are polar and terminate with Cd atoms, forming abundant adsorption sites for dioxygen-derived oxygen atoms.[48] On

This journal is © The Royal Society of Chemistry 2015

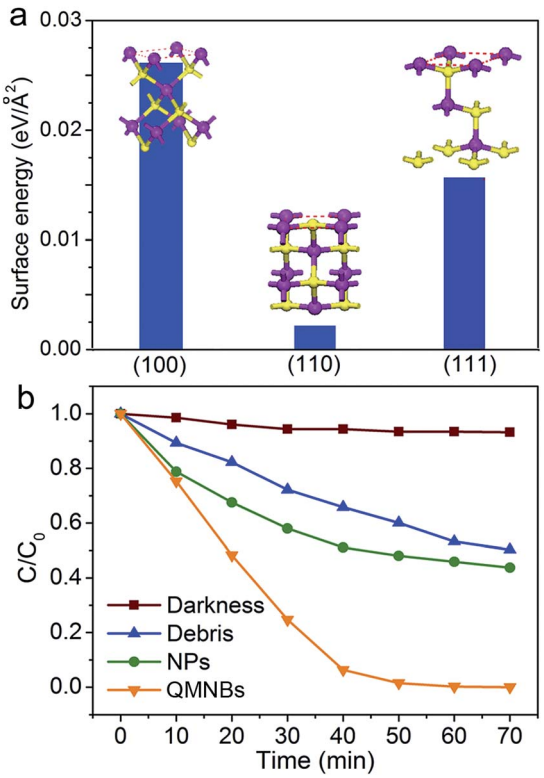

Fig. 6 Surface energy and photocatalytic activity of CdS QMNBs. (a) Surface energies for three facets of zinc-blende CdS. (b) Photocatalytic decay of MB by CdS nanoboxes, NPs and debris. The intensity change of MB absorption at 663 nm was recorded at different light-irradiation times. All samples were treated with EDA prior to mixing with MB solution and measured under the same conditions.

the other hand, the {100} planes exhibit high surface energy (0.02657 eV Å^{-2}), in favour of the degradation of organic molecules. The two factors jointly contribute to the enhanced photocatalytic activity of QMNBs.

Conclusions

In summary, we have demonstrated that the synergic reaction synthesis strategy combining the merits of cation exchange and chemical etching can generate diverse hollow nanostructures. More importantly, we found that the obtained CdS QMNBs have a metastable phase, exposed high-energy facets, the smallest size reported so far, and a rather large specific surface area, which jointly provide promising and exceptional catalytic activities. Our results demonstrate the power of synergic reactions in engineering of complex nanostructures with high quality and superior properties.

Acknowledgements

This work was supported by the National Basic Research Program of China (2014CB931703) and the Natural Science Foundation of China (Nos. 51171127, 51102176, and 51271129). Research carried out in part at the Center for Functional Nanomaterials, Brookhaven National Laboratory, which is supported by the U.S. Department of Energy, Office of Basic Energy Sciences, under Contract No. DE-AC02-98CH10886.

References

1 K. An and T. Hyeon, *Nano Today*, 2009, **4**, 359–373.
2 F. Xu, Z. Tang, S. Huang, L. Chen, Y. Liang, W. Mai, H. Zhong, R. Fu and D. Wu, *Nat. Commun.*, 2015, **6**, 7221.
3 C. Chen, Y. J. Kang, Z. Y. Huo, Z. W. Zhu, W. Y. Huang, H. L. L. Xin, J. D. Snyder, D. G. Li, J. A. Herron, M. Mavrikakis, M. F. Chi, K. L. More, Y. D. Li, N. M. Markovic, G. A. Somorjai, P. D. Yang and V. R. Stamenkovic, *Science*, 2014, **343**, 1339–1343.
4 X. Y. Yu, H. B. Wu, L. Yu, F. X. Ma and X. W. D. Lou, *Angew. Chem., Int. Ed.*, 2015, **54**, 4001–4004.
5 X. W. Lou, L. A. Archer and Z. Yang, *Adv. Mater.*, 2008, **20**, 3987–4019.
6 J. G. Yu, H. Guo, S. A. Davis and S. Mann, *Adv. Funct. Mater.*, 2006, **16**, 2035–2041.
7 Z. A. Huang, Z. Wang, K. Lv, Y. Zheng and K. Deng, *ACS Appl. Mater. Interfaces*, 2013, **5**, 8663–8669.
8 Z. Wang, D. Luan, F. Y. C. Boey and X. W. Lou, *J. Am. Chem. Soc.*, 2011, **133**, 4738–4741.
9 J. W. Nai, Y. Tian, X. Guan and L. Guo, *J. Am. Chem. Soc.*, 2013, **135**, 16082–16091.
10 C.-H. Kuo, Y.-T. Chu, Y.-F. Song and M. H. Huang, *Adv. Funct. Mater.*, 2011, **21**, 792–797.
11 E. Gonzalez, J. Arbiol and V. F. Puntes, *Science*, 2011, **334**, 1377–1380.
12 P. Afanasiev, *J. Phys. Chem. C*, 2012, **116**, 2371–2381.
13 L. Zhang, H. B. Wu and X. W. Lou, *J. Am. Chem. Soc.*, 2013, **135**, 10664–10672.
14 L. Zhang, L. Zhou, H. B. Wu, R. Xu and X. W. Lou, *Angew. Chem., Int. Ed.*, 2012, **51**, 7267–7270.
15 L. Tian, X. Yang, P. Lu, I. D. Williams, C. Wang, S. Ou, C. Liang and M. Wu, *Inorg. Chem.*, 2008, **47**, 5522–5524.
16 H. G. Yang and H. C. Zeng, *J. Phys. Chem. B*, 2004, **108**, 3492–3495.
17 P. H. C. Camargo, Y. H. Lee, U. Jeong, Z. Q. Zou and Y. N. Xia, *Langmuir*, 2007, **23**, 2985–2992.
18 J. B. Rivest and P. K. Jain, *Chem. Soc. Rev.*, 2013, **42**, 89–96.
19 S. K. Apte, S. N. Garaje, G. P. Mane, A. Vinu, S. D. Naik, D. P. Amalnerkar and B. B. Kale, *Small*, 2011, **7**, 957–964.
20 Z. Fang, Y. F. Liu, Y. T. Fan, Y. H. Ni, X. W. Wei, K. B. Tang, J. M. Shen and Y. Chen, *J. Phys. Chem. C*, 2011, **115**, 13968–13976.
21 Q. Li, B. D. Guo, J. G. Yu, J. R. Ran, B. H. Zhang, H. J. Yan and J. R. Gong, *J. Am. Chem. Soc.*, 2011, **133**, 10878–10884.
22 J. S. Jang, U. A. Joshi and J. S. Lee, *J. Phys. Chem. C*, 2007, **111**, 13280–13287.
23 Y. Yang, Y. Zheng, W. Cao, A. Titov, J. Hyvonen, J. R. Manders, J. Xue, P. H. Holloway and L. Qian, *Nat. Photonics*, 2015, **9**, 259–266.
24 P. F. Yin, T. Ling, Y. R. Lu, Z. W. Xu, S. Z. Qiao and X. W. Du, *Adv. Mater.*, 2015, **27**, 740–745.
25 T. Y. Zhai, X. S. Fang, L. Li, Y. Bando and D. Golberg, *Nanoscale*, 2010, **2**, 168–187.

26 T. Ling, S. A. Kulinich, Z. L. Zhu, S. Z. Qiao and X. W. Du, *Adv. Funct. Mater.*, 2014, **24**, 707–715.
27 D. Xu, Z. P. Liu, J. B. Liang and Y. T. Qian, *J. Phys. Chem. B*, 2005, **109**, 14344–14349.
28 R. M. Ma, X. L. Wei, L. Dai, H. B. Huo and G. G. Qin, *Nanotechnology*, 2007, **18**, 205605.
29 A. B. Panda, G. Glaspell and M. S. El-Shall, *J. Am. Chem. Soc.*, 2006, **128**, 2790–2791.
30 N. Z. Bao, L. M. Shen, T. Takata and K. Domen, *Chem. Mater.*, 2008, **20**, 110–117.
31 Y. Y. Huang, F. Q. Sun, H. J. Wang, Y. He, L. S. Li, Z. X. Huang, Q. S. Wu and J. C. Yu, *J. Mater. Chem.*, 2009, **19**, 6901–6906.
32 Y. X. Li, Y. F. Hu, S. Q. Peng, G. X. Lu and S. B. Li, *J. Phys. Chem. C*, 2009, **113**, 9352–9358.
33 R. M. Ma, L. Dai, H. B. Huo, W. Q. Yang, G. G. Qin, P. H. Tan, C. H. Huang and J. Zheng, *Appl. Phys. Lett.*, 2006, **89**, 203120.
34 N. Zhang, M. Q. Yang, Z. R. Tang and Y. J. Xu, *ACS Nano*, 2014, **8**, 623–633.
35 Y. Hu, Y. Liu, H. S. Qian, Z. Q. Li and J. F. Chen, *Langmuir*, 2010, **26**, 18570–18575.
36 Y. C. Cao and J. H. Wang, *J. Am. Chem. Soc.*, 2004, **126**, 14336–14337.
37 H. Tong, S. X. Ouyang, Y. P. Bi, N. Umezawa, M. Oshikiri and J. H. Ye, *Adv. Mater.*, 2012, **24**, 229–251.
38 R. Banerjee, R. Jayakrishnan and P. Ayyub, *J. Phys.: Condens. Matter*, 2000, **12**, 10647–10654.
39 J. Joo, H. B. Na, T. Yu, J. H. Yu, Y. W. Kim, F. X. Wu, J. Z. Zhang and T. Hyeon, *J. Am. Chem. Soc.*, 2003, **125**, 11100–11105.
40 J. P. Perdew, K. Burke and M. Ernzerhof, *Phys. Rev. Lett.*, 1996, **77**, 3865–3868.
41 D. Rodic, V. Spasojevic, A. Bajorek and P. Onnerud, *J. Magn. Magn. Mater.*, 1996, **152**, 159–164.
42 E. M. Chan, M. A. Marcus, S. Fakra, M. ElNaggar, R. A. Mathies and A. P. Alivisatos, *J. Phys. Chem. A*, 2007, **111**, 12210–12215.
43 M. Casavola, M. A. van Huis, S. Bals, K. Lambert, Z. Hens and D. Vanmaekelbergh, *Chem. Mater.*, 2012, **24**, 294–302.
44 X. Q. Gong and A. Selloni, *J. Phys. Chem. B*, 2005, **109**, 19560–19562.
45 X. Q. Gong, A. Selloni, M. Batzill and U. Diebold, *Nat. Mater.*, 2006, **5**, 665–670.
46 J. Pan, G. Liu, G. Q. Lu and H.-M. Cheng, *Angew. Chem., Int. Ed.*, 2011, **50**, 2133–2137.
47 H. Zhang, X. J. Lv, Y. M. Li, Y. Wang and J. H. Li, *ACS Nano*, 2010, **4**, 380–386.
48 W.-S. Wang, D.-H. Wang, W.-G. Qu, L.-Q. Lu and A.-W. Xu, *J. Phys. Chem. C*, 2012, **116**, 19893–19901.

This journal is © The Royal Society of Chemistry 2015